Electronic Supplementary Information for…

The Intrinsic Basicity of the Phosphate Backbone Exceeds that of Uracil and Thymine Residues: Protonation of the Phosphate Moiety is Preferred over the Nucleobase for pdThd and pUrd

R. R. Wu,[1] L. A. Hamlow,[1] C. C. He,[1] Y.-w. Nei,[1] G. Berden,[2] J. Oomens,[2] and M. T. Rodgers*[1]

Discussion

Comparison of Experimental IRMPD and Theoretical IR Spectra of $[\mathrm{pdThd+H}]^+$. The measured IRMPD and calculated IR spectra of the **PD**, **PE**, **TB**, **PF**, **TC**, and **O4B** of $[\mathrm{pdThd+H}]^+$ are compared in Figure S3 over the IR fingerprint and hydrogen-stretching regions. Mismatches between the measured and calculated spectra are highlighted. The highly anharmonic IRMPD features measured below ~1650 cm^{-1} in the fingerprint region are extensively broadened and thus not diagnostic. The calculated band at 1800 cm^{-1} of the **O4B** conformer is shifted to a higher frequency relative to the measured band at 1768 cm^{-1}. The calculated bands at 3583, 3595, 3581 and 3615 cm^{-1} of **PD**, **TB**, **TC** and **O4B**, respectively, are not observed in the measured spectrum. The calculated bands at 3669 and 3671 cm^{-1} of **TB** and **O4B**, respectively, are shifted to higher frequencies relative to the measured band at 3652 cm^{-1}. The bands predicted at 3636 cm^{-1} for **PE** and **PF** are lower in frequency than the measured band at 3652 cm^{-1}. These obvious discrepancies observed between the measured and calculated bands indicate the absence of the **TB**, **PE**, **PF**, and **O4B** conformers in the experiments as well.

Comparison of Experimental IRMPD and Theoretical IR Spectra of $[\mathrm{pUrd+H}]^+$. The measured IRMPD and calculated IR spectra of the **Piii**, **Piv**, **PD**, **PE**, **TB**, **Ti** and **TC** conformers of $[\mathrm{pUrd+H}]^+$ are compared in Figure S4 over the IR fingerprint and hydrogen-stretching regions. Mismatches between the measured and calculated spectra are highlighted. Again, the IRMPD features measured below ~1650 cm^{-1} in the fingerprint region for all these seven conformers and the hydrogen-bond acceptor hydrogen-stretches predicted at 3685 cm^{-1} for **Piii**, **Piv**, **PD**, **PE** and **TC** are not diagnostic due to their anharmonicities. The bands predicted at 3636 cm^{-1} for **Piii**,

---

[1] *Department of Chemistry, Wayne State University, Detroit, Michigan 48202, USA.*
E-mail:mrodgers@chem.wayne.edu: Tel +1 (313)577-2431
[2] *Radboud University, Institute for Molecules and Materials, FELIX Laboratory, Toernooiveld 7c, 6525 ED, Nijmegen, The Netherlands*

Piv and **PE** are lower in frequency than the measured band at 3652 cm^{-1}. The small IRMPD features predicted at 3615 and 3619 cm^{-1} for **Piv** and **Ti** respectively are higher in frequency than the weak band observed at 3588 cm^{-1}. The broad band predicted at 3666 cm^{-1} for **TB** is higher in frequency than the measured band at 3652 cm^{-1}. The calculated bands at 3579 cm^{-1} of **PD**, **Ti** and **TC** are lower in frequency than the measured band at 3588 cm^{-1}. The modest and broad band predicted at 3588 for TB matches the band position of the weak band observed at 3588 cm^{-1}. However, it is too intense relative to that of the measured band. Therefore, the discrepancies between the measured and calculated spectra particularly in the hydrogen-stretching region suggest that the **Piii**, **Piv**, **PD**, **PE**, **TB**, **Ti** and **TC** conformers are not populated in the experiments.

The measured IRMPD and calculated IR spectra of the **Pv**, **PF**, **Tii**, **O4B**, **O4i**, **Tiii** and **O2i** conformers of $[\mathrm{pUrd+H}]^+$ are compared in Figure S5 over the IR fingerprint and hydrogen-stretching regions. Mismatches between the measured and calculated spectra are highlighted. The IRMPD features measured below ~1650 cm^{-1} in the fingerprint region for all seven conformers and the hydrogen-bond acceptor hydrogen-stretches predicted at 3685 cm^{-1} for **Pv** and **PF**, and at 3678 cm^{-1} for **Tiii** and **O2i** are again not diagnostic. The strong IR feature predicted at 1822 cm^{-1} for **PF** is not observed in the measured spectrum. The calculated bands at 1814 and 1822 cm^{-1} of **O4B** and **O4i** respectively are higher in frequency than the measured band at 1797 cm^{-1}. The calculated bands at 3632 cm^{-1} of **Pv** and **PF** are lower in frequency than the band observed at 3652 cm^{-1}. The calculated IR bands in the hydrogen-stretching regions of the **Tii**, **O4B**, **O4i**, **Tiii** and **O2i** conformers exhibit very distinct differences as compared to the measured IRMPD bands. In particular, the bands predicted at 3670 cm^{-1} for **Tii**, **O4B** and **O4i** are higher in frequency than the measured band at 3652 cm^{-1}. The IR features predicted at 3627 cm^{-1} for **Tii**, **O4B** and **O4i** are not observed in the measured spectrum. The band predicted at 3691 cm^{-1} for **Tii** is too intense relative to the small measured band at that vibrational frequency. The calculated bands at 3519 and 3504 cm^{-1} of **Tiii** and **O2i** are not observed in the measured spectrum. Therefore, the discrepancies between the measured and calculated spectra particularly in the hydrogen-stretching region suggest that the **Pv**, **PF**, **Tii**, **O4B**, **O4i**, **Tiii** and **O2i** conformers are not populated in the experiments.

Table S1. Relative Enthalpies and Free Energies at 0 and 298 K in kJ/mol of Select Low-Energy Conformers of [pdThd+H]$^+$ and [pUrd+H]$^+$ in a Polarizable Continuum[a]

Species	Conformer	MP2(full)			B3LYP		
		ΔH_0	ΔH_{298}	ΔG_{298}	ΔH_0	ΔH_{298}	ΔG_{298}
[pdThd+H]$^+$	**PA**[b]	**0.0**	**0.0**	0.2	**0.0**	**0.0**	0.8
	PB[b]	2.1	2.5	**0.0**	1.5	1.9	**0.0**
	PC	15.1	14.4	17.1	4.5	3.8	7.1
	TA	28.5	28.5	28.1	24.2	24.1	24.3
	O2A[b]	16.0	11.6	24.8	5.9	1.5	15.3
	O4A	25.2	24.0	26.7	14.6	13.4	16.7
[pdUrd+H]$^+$	**PA**[b]	**0.0**	0.3	2.1	0.3	0.8	10.4
	PB[b]	1.1	**0.0**	4.0	0.9	**0.0**	11.8
	PC	8.0	12.2	**0.0**	**0.0**	4.4	**0.0**
	TA	25.1	26.8	23.5	21.4	23.3	27.9
	O4A	21.1	20.2	22.4	10.2	9.5	19.4

[a] Single point energy calculations using the B3LYP/6-311+G(d,p) optimized structures are performed at the MP2(full)/6-311+G(2d,2p) and B3LYP/6-311+G(2d,2p) levels of theory with the IEFPCM polarizable continuum model and include ZPE and thermal corrections. The relative stabilities of the ground conformers are indicated in boldface. [b] Low-energy conformers that are populated in the gas phase and contribute to the measured IRMPD action spectra.

Figure Captions

Figure S1. B3LYP/6-311+G(d,p) low-energy conformers of [pdThd+H]$^+$ and their relative Gibbs free energies at 298 K calculated at the MP2(full)/6-311+G(2d,2p) (in red) and B3LYP/6-311+G(2d,2p) (in black) levels of theory. The site of protonation/tautomeric form, nucleobase orientation, and sugar puckering are also indicated for each conformer.

Figure S2. B3LYP/6-311+G(d,p) low-energy conformers of [pUrd+H]$^+$ and their relative Gibbs free energies at 298 K calculated at the MP2(full)/6-311+G(2d,2p) (in red) and B3LYP/6-311+G(2d,2p) (in black) levels of theory. The site of protonation/tautomeric form, nucleobase orientation, and sugar puckering are also indicated for each conformer.

Figure S3. Comparison of the measured IRMPD action spectrum of $[\mathrm{pdThd{+}H}]^+$ with the theoretical linear IR spectra of the **PD**, **PE**, **TB**, **PF**, **TC**, and **O4B** conformers of $[\mathrm{pdThd{+}H}]^+$ and the corresponding B3LYP/6-311+G(d,p) optimized structures. Also shown are the MP2(full)/6-311+G(2d,2p) (in red) and B3LYP/6-311+G(2d,2p) (in black) relative Gibbs free energies at 298 K. The site of protonation/tautomeric form, nucleobase orientation, and sugar puckering are also indicated for each conformer. To facilitate comparison of the measured and computed spectra, the IRMPD spectrum is overlaid (in grey) with each computed spectrum and scaled to match the intensity of the most intense feature in each region.

Figure S4. Comparison of the measured IRMPD action spectrum of $[\mathrm{pUrd{+}H}]^+$ with the theoretical linear IR spectra of the **Piii**, **Piv**, **PD**, **PE**, **TB**, **Ti** and **TC** conformers of $[\mathrm{pUrd{+}H}]^+$ and the corresponding B3LYP/6-311+G(d,p) optimized structures. Also shown are the MP2(full)/6-311+G(2d,2p) (in red) and B3LYP/6-311+G(2d,2p) (in black) relative Gibbs free energies at 298 K. The site of protonation/tautomeric form, nucleobase orientation, and sugar puckering are also indicated for each conformer. To facilitate comparison of the measured and computed spectra, the IRMPD spectrum is overlaid (in grey) with each computed spectrum and scaled to match the intensity of the most intense feature in each region.

Figure S5. Comparison of the measured IRMPD action spectrum of $[\mathrm{pUrd{+}H}]^+$ with the theoretical linear IR spectra of the **Pv**, **PF**, **Tii**, **O4B**, **O4i**, **Tiii** and **O2i** conformers of $[\mathrm{pUrd{+}H}]^+$ and the corresponding B3LYP/6-311+G(d,p) optimized structures. Also shown are the MP2(full)/6-311+G(2d,2p) (in red) and B3LYP/6-311+G(2d,2p) (in black) relative Gibbs free energies at 298 K. The site of protonation/tautomeric form, nucleobase orientation, and sugar puckering are also indicated for each conformer. To facilitate comparison of the measured and computed spectra, the IRMPD spectrum is overlaid (in grey) with each computed spectrum and scaled to match the intensity of the most intense feature in each region.

Figure S1.

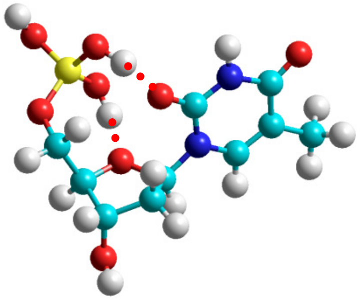

PA, syn, C2'-endo
0.0, 0.7 kJ/mol

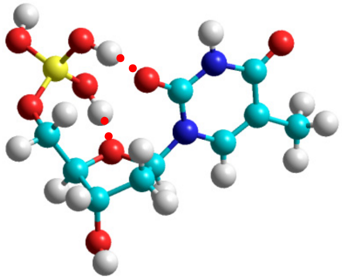

PB, syn, C2'-endo
0.2, 0.3 kJ/mol

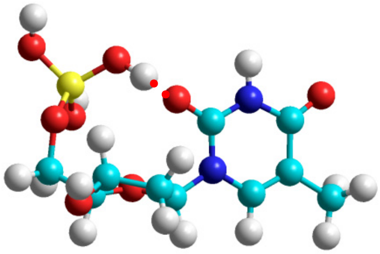

PC, syn, C3'-endo
10.6, 0.0 kJ/mol

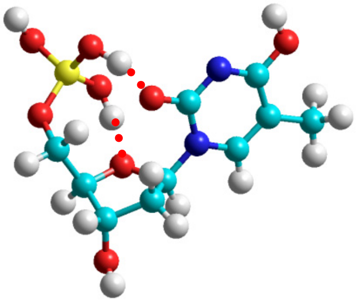

PD, syn, C2'-endo
11.1, 15.2 kJ/mol

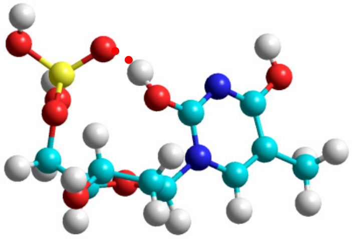

TA, syn, C3'-endo
11.7, 4.3 kJ/mol

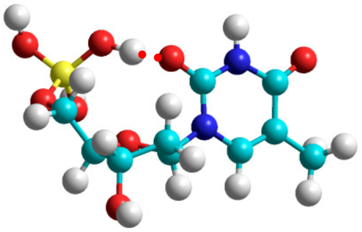

PE, syn, C2'-endo
11.7, 5.2 kJ/mol

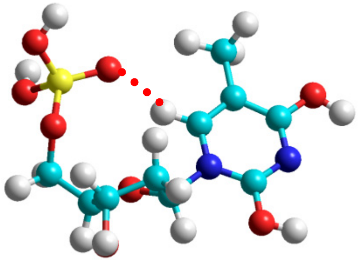

TB, anti, C2'-endo
11.8, 7.9 kJ/mol

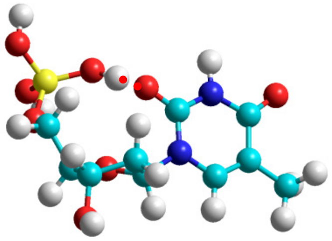

PF, syn, C2'-endo
12.4, 2.3 kJ/mol

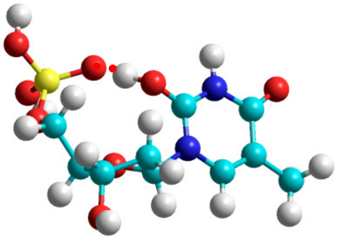

O2A, syn, C2'-endo
13.0, 2.9 kJ/mol

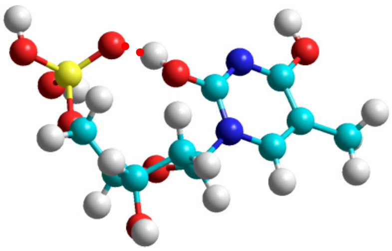

TC, syn, C2'-endo
14.4, 9.0 kJ/mol

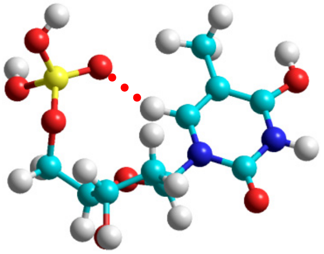

O4A, anti, C2'-endo
18.7, 6.4 kJ/mol

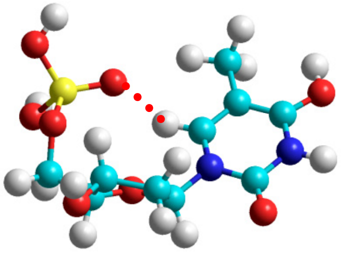

O4B, anti, C3'-endo
24.8, 9.8 kJ/mol

$[pdThd+H]^+$

Figure S2.

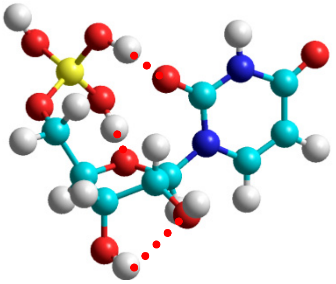

Pi, syn, C2'-endo
0.0, 3.9 kJ/mol

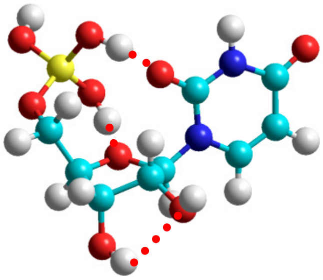

Pii, syn, C2'-endo
0.2, 3.5 kJ/mol

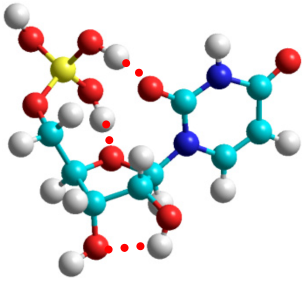

PA, syn, C2'-endo
4.2, 7.0 kJ/mol

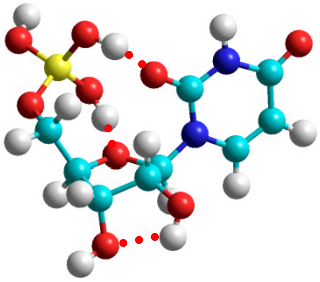

PB, syn, C2'-endo
5.0, 7.3 kJ/mol

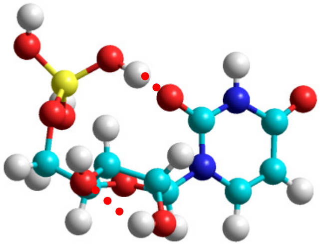

PC, syn, C3'-endo
6.0, 0.0 kJ/mol

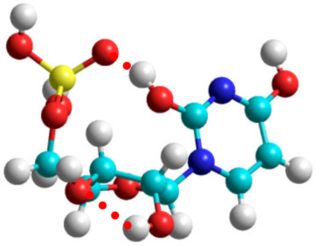

TA, syn, C3'-endo
7.3, 2.1 kJ/mol

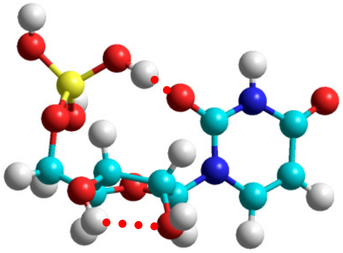

Piii, syn, C3'-endo
9.7, 2.2 kJ/mol

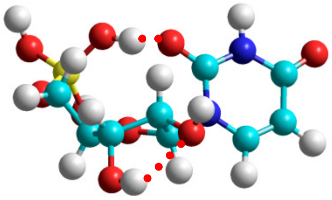

Piv, syn, C2'-endo
10.8, 8.1 kJ/mol

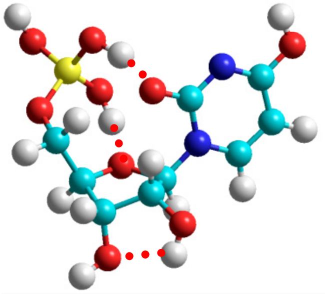

PD, syn, C2'-endo
11.9, 16.5 kJ/mol

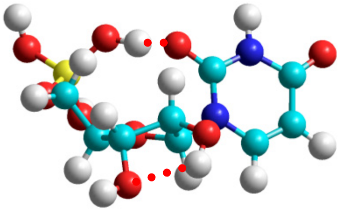

PE, syn, C2'-endo
13.0, 8.1 kJ/mol

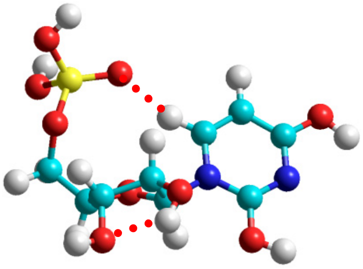

TB, anti, C2'-endo
13.1, 8.8 kJ/mol

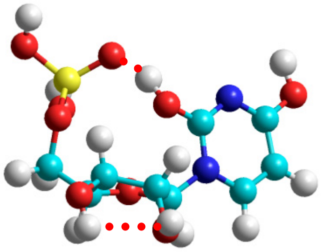

Ti, syn, C3'-endo
13.4, 8.4 kJ/mol

[pUrd+H]$^+$

Figure S2.

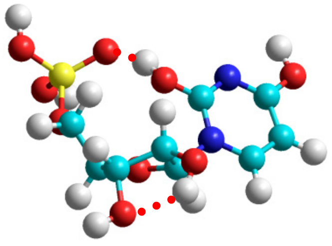

TC, syn, C2'-endo
13.7, 6.9 kJ/mol

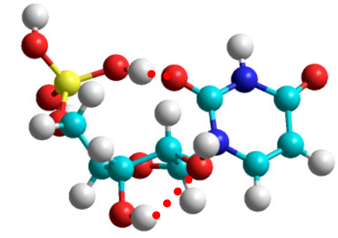

Pv, syn, C2'-endo
14.6, 9.2 kJ/mol

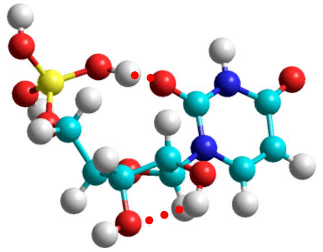

PF, syn, C2'-endo
15.8, 8.2 kJ/mol

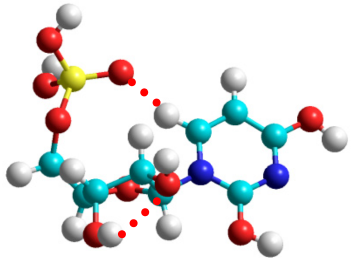

Tii, anti, C2'-endo
15.9, 14.0 kJ/mol

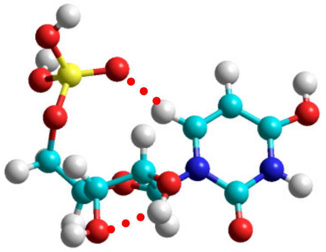

O4A, anti, C2'-endo
18.1, 6.5 kJ/mol

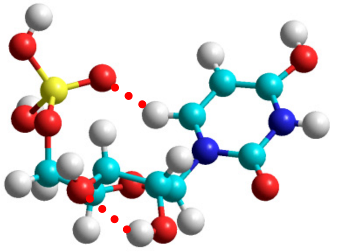

O4B, anti, C3'-endo
23.3, 11.6 kJ/mol

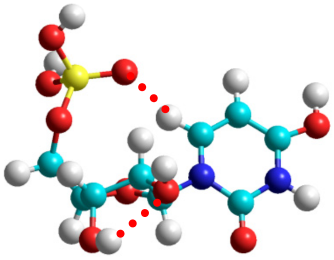

O4i, anti, C2'-endo
23.5, 14.2 kJ/mol

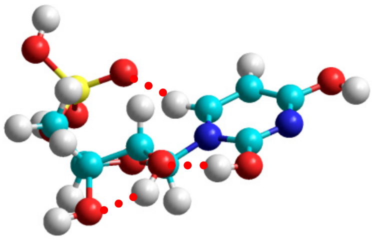

Tiii, anti, C2'-endo
27.5, 20.8 kJ/mol

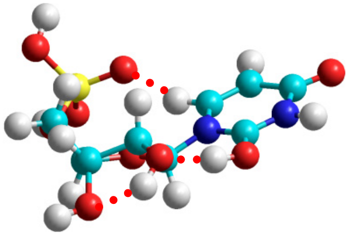

O2i, anti, C2'-endo
39.1, 32.2 kJ/mol

$[\mathrm{pUrd+H}]^+$

Figure S3.

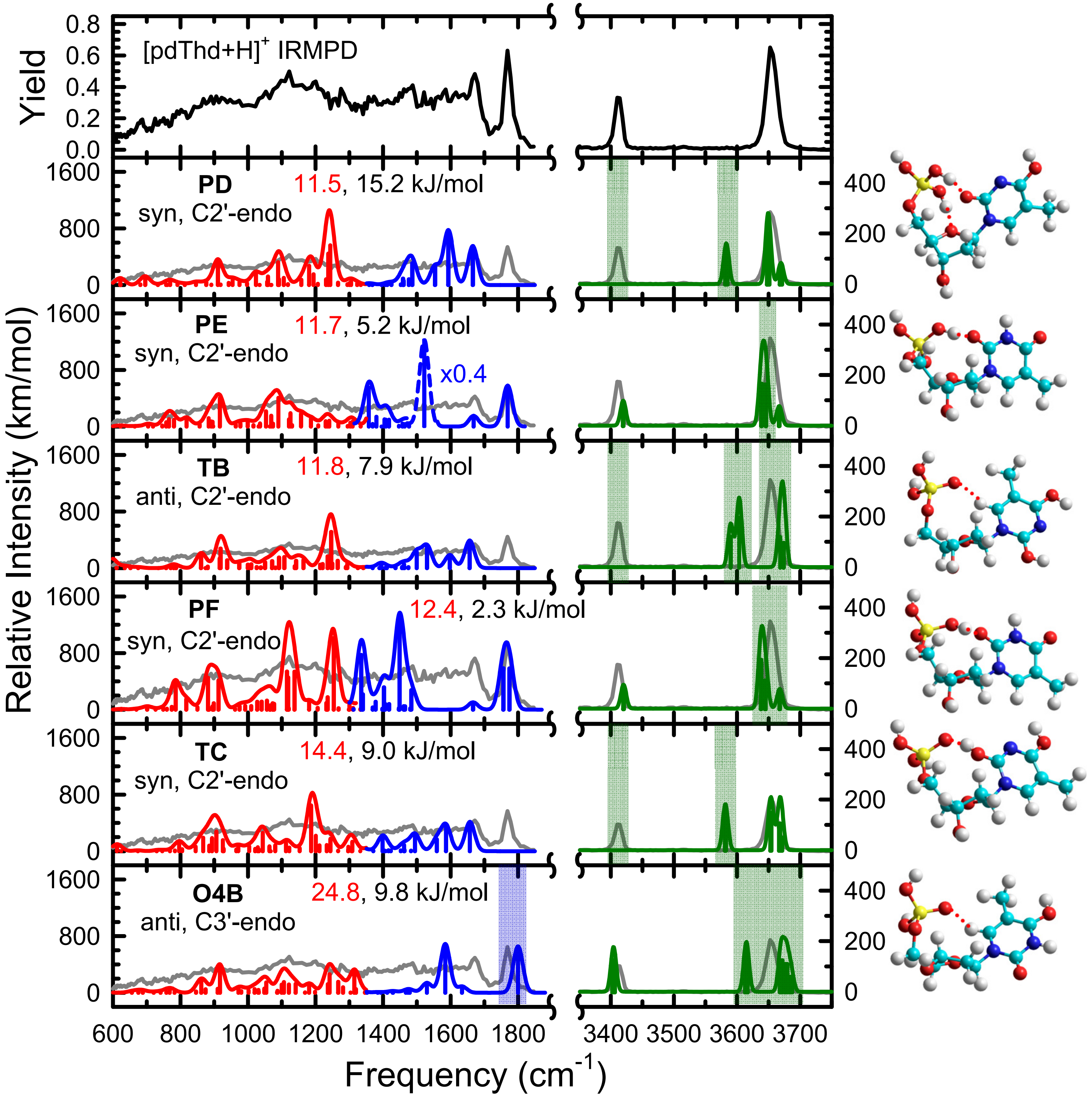
[pdThd+H]$^+$ IRMPD
Yield
0.8
0.6
0.4
0.2
0.0
PD
11.5, 15.2 kJ/mol
syn, C2'-endo
PE
11.7, 5.2 kJ/mol
syn, C2'-endo
x0.4
TB
11.8, 7.9 kJ/mol
anti, C2'-endo
PF
12.4, 2.3 kJ/mol
syn, C2'-endo
TC
14.4, 9.0 kJ/mol
syn, C2'-endo
O4B
24.8, 9.8 kJ/mol
anti, C3'-endo
Relative Intensity (km/mol)
1600
800
0
400
200
0
600
800
1000
1200
1400
1600
1800
3400
3500
3600
3700
Frequency (cm^{-1})

Figure S4.

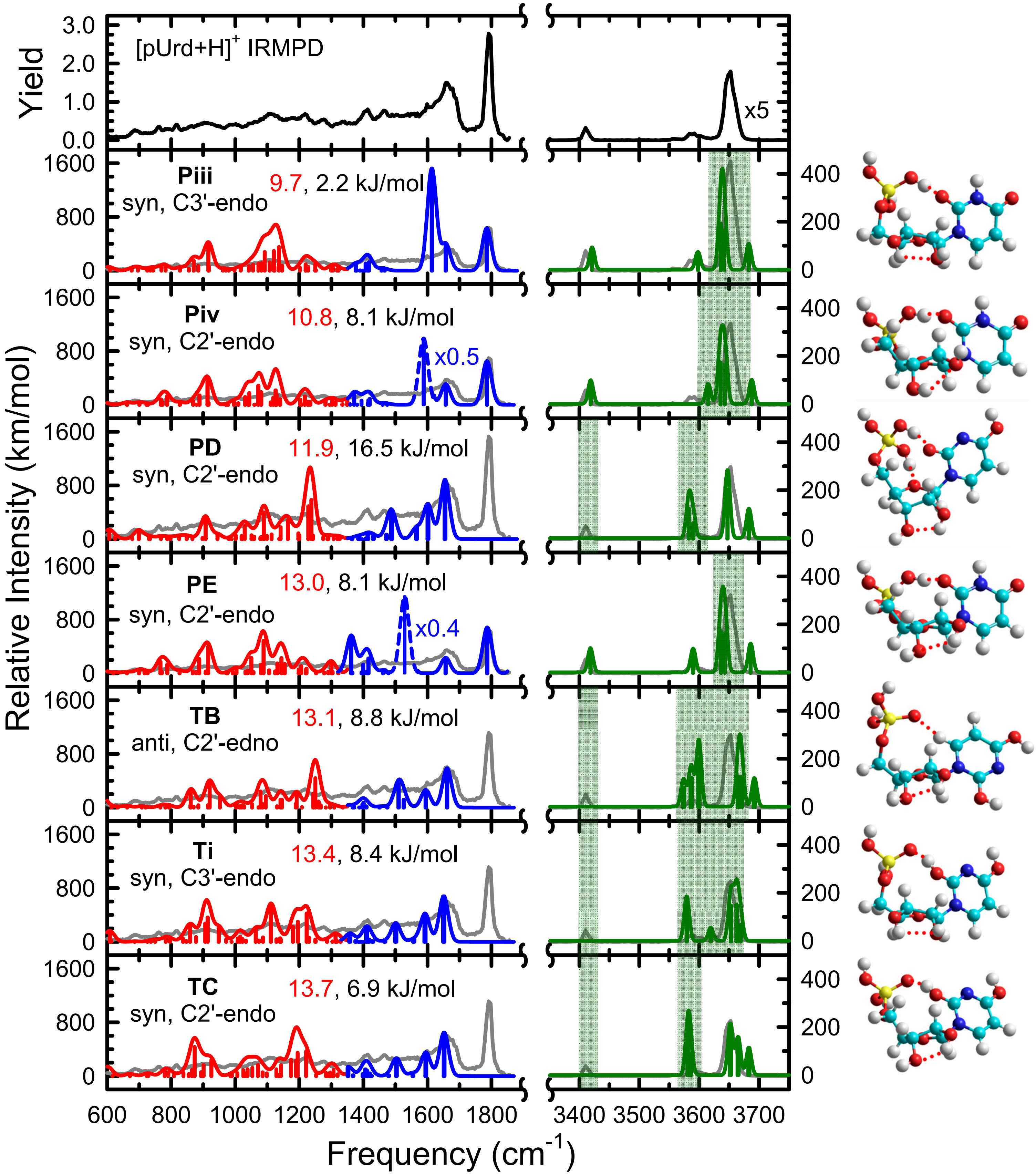
[pUrd+H]+ IRMPD
Yield
3.0
2.0
1.0
0.0
x5
Piii
syn, C3'-endo
9.7, 2.2 kJ/mol
Piv
syn, C2'-endo
10.8, 8.1 kJ/mol
x0.5
PD
syn, C2'-endo
11.9, 16.5 kJ/mol
PE
syn, C2'-endo
13.0, 8.1 kJ/mol
x0.4
TB
anti, C2'-edno
13.1, 8.8 kJ/mol
Ti
syn, C3'-endo
13.4, 8.4 kJ/mol
TC
syn, C2'-endo
13.7, 6.9 kJ/mol
1600
800
0
400
200
0
Relative Intensity (km/mol)
600
800
1000
1200
1400
1600
1800
3400
3500
3600
3700
Frequency (cm-1)

Figure S5.

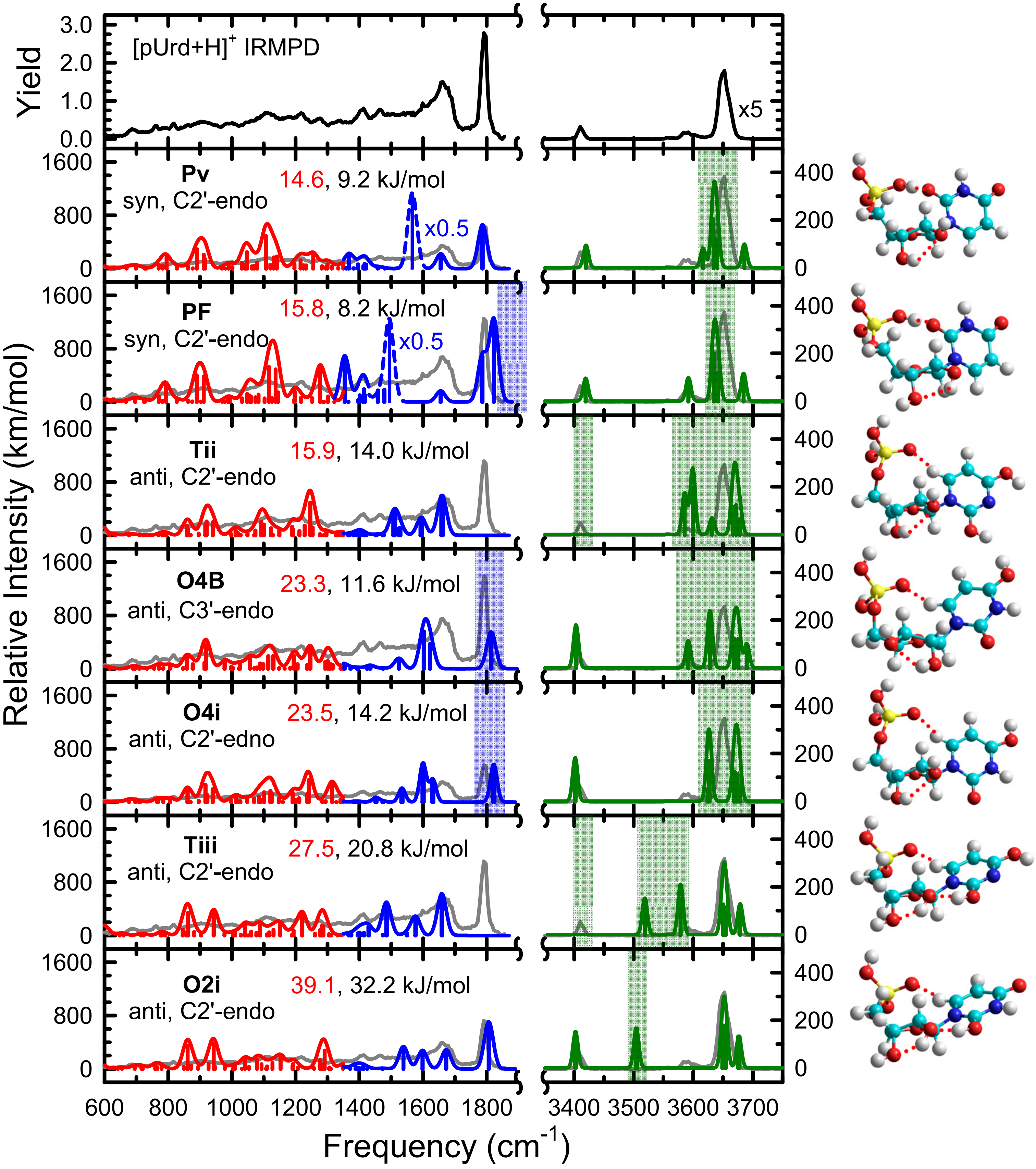
[pUrd+H]$^+$ IRMPD
x5
Yield
3.0
2.0
1.0
0.0
Pv
14.6, 9.2 kJ/mol
syn, C2'-endo
x0.5
PF
15.8, 8.2 kJ/mol
syn, C2'-endo
x0.5
Tii
15.9, 14.0 kJ/mol
anti, C2'-endo
O4B
23.3, 11.6 kJ/mol
anti, C3'-endo
O4i
23.5, 14.2 kJ/mol
anti, C2'-edno
Tiii
27.5, 20.8 kJ/mol
anti, C2'-endo
O2i
39.1, 32.2 kJ/mol
anti, C2'-endo
Relative Intensity (km/mol)
1600
800
0
400
200
0
600
800
1000
1200
1400
1600
1800
3400
3500
3600
3700
Frequency (cm^{-1})